Black-box decomposition approach for computational hemodynamics: One-dimensional models

P.J. Blanco[a,d,*], J.S. Leiva[b], R.A. Feijóo[a,d], G.C. Buscaglia[c,d]

[a] *Laboratório Nacional de Computação Científica, Av. Getúlio Vargas 333, Quitandinha, 25651–075, Petrópolis, RJ, Brazil, pjblanco@lncc.br, feij@lncc.br*
[b] *Instituto Balseiro, Av. Bustillo Km. 9.5, San Carlos de Bariloche, 8400, Río Negro, Argentina, leivaj@ib.cnea.gov.ar*
[c] *Instituto de Ciências Matemáticas e Computação, Universidade de São Paulo, Av. do Trabalhador Sãocarlense 400, 13560-970 São Carlos, SP, Brazil*
[d] *Instituto Nacional de Ciência e Tecnologia em Medicina Assistida por Computação Científica, Brazil*

Abstract

Increasing efforts exist in integrating different levels of blood circulation in models of the cardiovascular system. In this context, effective and black-box-type decomposition strategies for one-dimensional networks are needed, so as to: (i) employ domain decomposition strategies for large systemic models (1D-1D coupling) and (ii) provide the conceptual basis for dimensionally-heterogeneous representations (1D-3D coupling, among various possibilities). The strategy proposed in this article works for both of these two scenarios, though the several applications shown to illustrate its behavior focus on the 1D-1D coupling case.

The network is decomposed in such a way that each coupling point connects two (and not more) of the sub-networks. At each of the M connection points two unknowns are defined: the flow rate and pressure. These $2M$ unknowns are determined by $2M$ equations, since each sub-network provides one (nonlinear) equation per coupling point. It is shown how to build the $2M \times 2M$ nonlinear system with arbitrary and independent choice of boundary conditions for each of the sub-networks. The idea is then to solve this nonlinear system until convergence, which guarantees *strong coupling* of the complete network. In other words, *if the nonlinear solver converges at each time step*, the solution coincides with what would be obtained by monolithically modelling the whole network. The decomposition thus imposes no stability restriction on the choice of the time step size.

Effective iterative strategies for the nonlinear system that preserve the black-box character of the decomposition are then explored. Several variants of matrix-free Broyden's and Newton-GMRES algorithms are assessed as numer-

*Corresponding author.
Email addresses: pjblanco@lncc.br. Tel:+55 24 22336067, fax:+55 24 22336071 (P.J. Blanco)

ical solvers by comparing their performance on sub-critical wave propagation problems which range from academic test cases to realistic cardiovascular applications. A specific variant of Broyden's algorithm is identified and recommended on the basis of its computer cost and reliability.

Key words: Partitioned analysis, Hemodynamics, 1D models, Domain decomposition, Wave propagation.

---

1. Introduction

Modeling different physical phenomena within the cardiovascular system has become a priority for the scientific community of computational modeling and numerical simulation. When analyzing global quantities in the whole arterial network and virtual scenarios of the cardiovascular system, 1D (and also 0D) models have proven to be the most convenient in terms of the trade-off between predictive capabilities and computational cost [1, 2, 3, 4, 5, 6, 7, 8, 9, 10, 11, 12, 13, 14, 15, 16].

Usually, these simple models involve a small number of unknowns and the computational cost is not a barrier. However, recent contributions [10] addressing capillary circulation have posed the problem of setting-up block-partitioned analyses in order to apply upscaling techniques. Moreover, the data acquisition technology employed nowadays allows to set up quite detailed topological structures of the cardiovascular system, so that the analysis of very complex, patient-specific networks will soon be routine both in its direct (analysis) and inverse (parameter estimation [17, 18]) forms.

Another important problem arises when putting together heterogeneous models to simulate different components of the whole network. Models for the venous or pulmonary circulation, models for the heart-valvular functioning, or models for the capillary circulation, among others, are self-speaking examples. Coupling such models may be a cumbersome task if they, for instance, are originally implemented in different codes or even if they belong to different research groups. In this sense, having a systematic approach to couple such heterogeneous models using a black-box concept will hopefully contribute to speed up research in this area.

The aim of this article is to introduce a systematic approach to set up iterative strategies to decouple one-dimensional flow models into sub-networks. This is accomplished by recasting the original problem in terms of interface variables, specifically the pressure and flow rate at each of the M coupling points, leading to $2M$ unknowns. It is assumed that each point couples two (and not more) sub-networks. Since the dynamical equations of each sub-network provide one equation per coupling point, these equations can be assembled into a closed $2M \times 2M$ nonlinear system. In the proposed approach the boundary conditions can be chosen arbitrarily for each sub-network, so that a black-box strategy can indeed be implemented. For the numerical treatment of the nonlinear system, we adopt Broyden's and Newton-GMRES techniques, assessing

the performance of each variant. Indeed, any Jacobian-free method could be applied. In this stage of the research we will not focus on the gains regarding CPU time, nor in the comparison between iterative and monolithic approaches.

The strategies developed here are envisaged for sub-critical flows, i.e., for fluid velocities smaller than the characteristic velocity. This is fully justified in hemodynamics, since the fluid velocity hardly exceeds one tenth of the characteristic velocity. In the super-critical regime the choice of boundary conditions for the sub-networks is severely restricted, since there may be no information traveling upstream.

The proposed methodology stems from the ideas developed in [19] to deal with the coupling of 3D–1D models in linear problems. In the simplest case of two sub-networks converging to a coupling point, we arrive at the interface problem by (a) keeping the unknowns for which some continuity condition must be enforced (two in the present case, flow rate and pressure) and (b) writing the corresponding (two) equations provided by each of the underlaying sub-networks. This strategy differs from classical domain decomposition approaches, since it makes use of the two unknowns instead of reducing the problem to a single unknown, namely a primal approach (Steklov-Poincaré equation), or a dual approach (FETI equation). With this not only we gain versatility in setting boundary conditions for the different underlaying sub-networks, as stated in the previous paragraph, but also allows for the black-box application of iterative solvers other than the classical Dirichlet-to-Neumann iterations and its variants [20, 21]. In fact, classical methods are shown to correspond to Gauss-Seidel iterations of the nonlinear system built by our methodology. We explore more sophisticated and robust solvers for systems of nonlinear equations, in particular Broyden's or Newton-GMRES methods, and identify a specific choice that is to be recommended for both its computer cost and its reliability.

This work is organized as follows: Section 2 gives an account of the governing equations and continuity conditions at the coupling points. In Section 3 the iterative strategies are presented, while in Section 4 these strategies are tested in academic examples. The application of the numerical methods to computational hemodynamics is addressed in Section 5, and some additional observations are pointed out in Section 6. Finally, the conclusions are drawn in Section 7.

2. Governing equations

2.1. Mathematical model

Blood flow in large arteries can be modeled using the condensed 1D Navier-Stokes equations in compliant vessels, which comprises momentum and mass conservation [22] as follows

$$\frac{\partial Q}{\partial t} + \frac{\partial}{\partial x}\left(\alpha_m \frac{Q^2}{A}\right) + \frac{A}{\rho}\frac{\partial P}{\partial x} + \frac{2\pi R}{\rho}\tau_o = 0, \tag{1}$$

$$\frac{\partial A}{\partial t} + \frac{\partial Q}{\partial x} = 0, \tag{2}$$

where A is the luminal area (and R is the radius), Q is the flow rate, P is the mean pressure, ρ is the density and τ_o accounts for the viscous effects since it is

$$\tau_o = f_r \frac{\rho U|U|}{8},$$

where U is the mean velocity ($U = Q/A$) and f_r is the Darcy friction factor corresponding to a fully-developed parabolic velocity profile. In this work the momentum correction factor α_m has been taken as equal to one. These hypotheses can be refined by introducing Womersley-like velocity profiles for the friction and momentum terms (see [11]). In the authors experience the influence of the correction factor is negligible, while the parabolic profile considered here may yield an underestimated pressure drop due to viscous dissipation in some cases. In any case, the conclusions of the present work should not be affected greatly when changing such hypotheses.

Equations (1)–(2) are complemented with a constitutive relation for the arterial wall relating the pressure with the cross sectional area. In this work the following independent-ring viscoelastic model (see [23, 24]) was used

$$P = P_0 + \frac{Eh}{R_0}\left(\sqrt{\frac{A}{A_0}} - 1\right) + \frac{Kh}{R_0}\frac{1}{2\sqrt{A_0 A}}\frac{\partial A}{\partial t}, \tag{3}$$

where index 0 refers to reference values, h is the wall thickness and E and K are the material parameters that characterize the elastic and viscoelastic material responses, respectively.

Recall that in the case of a pure elastic constitutive model (i.e. $K = 0$) a hyperbolic system of equations is recovered with wave celerities (eigenvalues) given by $\lambda_{1,2} = U \pm c$, with

$$c = \sqrt{\frac{A}{\rho}\frac{\partial P}{\partial A}}.$$

Regarding the boundary conditions to system (1)–(3), as long as the flow is subcritical ($|U| < c$) one boundary condition needs to be applied at each end of the vessel. The most common practice is to impose the flow rate Q or the pressure P independently at each end, depending on the physical setting, but imposing combinations of both Q and P is also possible.

2.2. Coupling conditions

Consider the simplest case of a network consisting of just one vessel, which is decomposed into two connected parts, so that each of the two sub-networks also consists of just one vessel. Extension to multicomponent systems is quite straightforward. Two coupling conditions arise at the coupling point C, see Figure 1, which can be written as

$$Q_1 = Q_2, \tag{4}$$
$$P_1 = P_2, \tag{5}$$

where 1 and 2 indicate the two partitions of the vessel. It is assumed that no jump in the cross sectional area takes place at the coupling point. Therefore, the mean velocity is also continuous ($U_1 = U_2$), as well as the total pressure; i.e.,

$$T_1 = \frac{1}{2}\rho U_1^2 + P_1 = \frac{1}{2}\rho U_2^2 + P_2 = T_2,$$

which can substitute either (4) or (5).

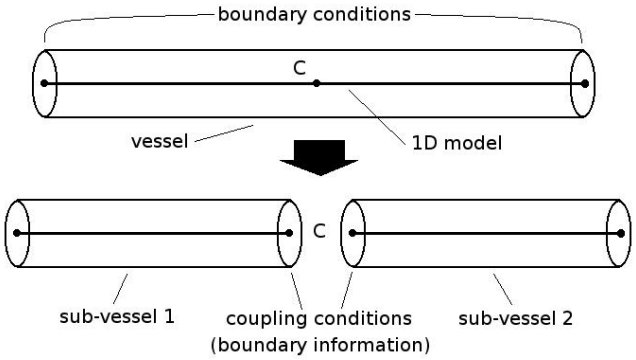

Figure 1: Decomposition of a simple vessel.

Note that in the case of a simple vessel each sub-network (each partition) has a unique coupling interface. In the case of a more complex network, as the one shown in Figure 2, the sub-networks may consist of many vessels and have several coupling interfaces. In any case, the decomposition is performed along single vessels (not at bifurcations, trifurcations, etc.) and therefore we have always two vessels arriving at each coupling interface.

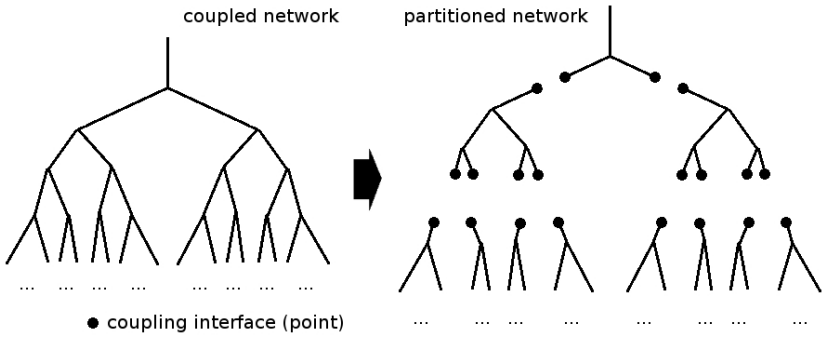

Figure 2: Decomposition of a network with sub-networks containing 1, 2 and 5 coupling interfaces (points).

3. Black-box decomposition approach

This section deals with the basic concepts behind the strategies proposed in the present work. They are based on our previous work [19].

3.1. Interface problem

Always referring to the simple case of Figure 1, the decomposition introduced four new unknowns (Q_1, Q_2, P_1, P_2), which are linked by the coupling equations (4)-(5), so that we are lacking two equations. These come from the individual responses of each sub-network. For sub-network 1, for example, not any combination of Q_1 and P_1 is feasible. More specifically, if some arbitrary value of P_1 is imposed as boundary condition at C, Q_1 is fully determined. Viceversa, if Q_1 is arbitrarily chosen and imposed as boundary condition, P_1 is determined by the unique solution of (1)–(3) in sub-network 1. Let us denote this dependence as $\mathcal{F}_1(Q_1, P_1) = 0$, and similarly for sub-network 2. The closed system thus reads

$$\begin{aligned} Q_1 &= Q_2, \\ P_1 &= P_2, \\ \mathcal{F}_1(Q_1, P_1) &= 0, \\ \mathcal{F}_2(Q_2, P_2) &= 0, \end{aligned}$$

which can be further simplified, denoting $Q = Q_1 = Q_2$ and $P = P_1 = P_2$, to

$$\mathcal{F}_1(Q, P) = 0, \tag{6}$$
$$\mathcal{F}_2(Q, P) = 0. \tag{7}$$

The flow rate and pressure at C correspond to a *state* of the system. The functions $\mathcal{F}_1$ and $\mathcal{F}_2$ need to be defined for any such state, and the solution of the interface problem is the unique state which makes (6)–(7) to hold. Notice that in this discussion we have disregarded the time dependence of the variables, since in practice the time will be discretized and the procedures described here will be used at each time step.

Let $(\tilde{Q}, \tilde{P})$ be an arbitrary state of the system. The state uniquely determines the corresponding area $\tilde{A}$ through the constitutive relation, as well as the velocity $\tilde{U} = \tilde{Q}/\tilde{A}$ and the total pressure $\tilde{T} = \frac{\rho}{2}\tilde{U}^2 + \tilde{P}$. The situation is similar to that of thermodynamics of gases, in which the thermodynamic state is fully determined by any two state variables. We will however, for the sake of clarity, only represent states as flow rate/pressure pairs. The nature of the functions $\mathcal{F}_1$ and $\mathcal{F}_2$ depends on the way boundary conditions at the coupling point are imposed for each sub-network:

- Assume that the flow-rate $\tilde{Q}$ is imposed at the coupling point for sub-network 1. Then, by solving (6) in this sub-network, a corresponding pressure is obtained, which can be denoted by $\mathcal{P}_{q,1}(\tilde{Q})$, meaning that it is the pressure obtained at point C when running subsystem 1 as a black box

with imposed flow-rate data at C given by $\tilde{Q}$. In this case, the function $\mathcal{F}_1$ is naturally given by

$$\mathcal{F}_1(\tilde{Q}, \tilde{P}) = \tilde{P} - \mathcal{P}_{q,1}(\tilde{Q}), \tag{8}$$

and evaluated at the exact solution (Q, P) it will be zero.

- Let us explain the procedure when pressure is imposed at C in the case of sub-network 2. If the imposed value is $\tilde{P}$, then running sub-network 2 as a black box with this boundary condition at C will yield some well-determined flow-rate at C, which is denoted by $\mathcal{Q}_{p,2}(\tilde{P})$, and the function $\mathcal{F}_2$ is given by

$$\mathcal{F}_2(\tilde{Q}, \tilde{P}) = \tilde{Q} - \mathcal{Q}_{p,2}(\tilde{P}),$$

which, combined with (8) would yield a closed system.

- It could well happen that one decides to run, say, sub-network 2 as a black box with the total pressure $\tilde{T}$ imposed at C, instead of the pressure or flow rate. This would yield both a flow rate $\mathcal{Q}_{t,2}(\tilde{T})$ and a pressure $\mathcal{P}_{t,2}(\tilde{T})$ at C as results. In this case the function $\mathcal{F}_2$ is chosen as

$$\mathcal{F}_2(\tilde{Q}, \tilde{P}) = \tilde{Q} - \mathcal{Q}_{t,2}(\tilde{T}(\tilde{Q}, \tilde{P})).$$

- Another choice would be $\mathcal{F}_2 = \tilde{P} - \mathcal{P}_{t,2}(\tilde{T})$, but we prefer the former because in the vicinity of $\tilde{Q} = 0$ the variables $\tilde{P}$ and $\tilde{T}$ are linearly dependent.

3.2. Time discretization

Before proceeding further, let us assume that a time discretization scheme is applied to the system of partial differential equations. In this way, the interface problem is formulated at each time step t^n through time-discrete operators $\mathcal{F}_1^n$ and $\mathcal{F}_2^n$ which encompass the dependencies with respect to the values of the unknowns at past time steps (Q^{n-1}, P^{n-1}), (Q^{n-2}, P^{n-2}), and so on. Then, given proper initial conditions (Q^0, P^0), equations (6)–(7) are replaced by the following time-discrete equations valid for each time step $n = 0, 1, 2, \ldots$

$$\mathcal{F}_1^n(Q^n, P^n) = 0, \tag{9}$$
$$\mathcal{F}_2^n(Q^n, P^n) = 0. \tag{10}$$

This is actually a system of two equations in the two unknowns (Q^n, P^n) which corresponds to the different equilibria formulated at the interface. Hence, at each time step, system (9)–(10) is assembled with the contribution of one equation from each arriving vessel. The solution of (9)–(10) leads to a fully-coupled (strongly coupled) strategy for advancement in time.

Remark 1. Since it is necessary to assemble a system of equations at each time step, the equations contributed by each vessel may change with time. Consider sub-vessel 1, in the first part of the simulation we could impose flow rate and in the rest of the simulation pressure, disregarding what happens in the complementary sub-domain.

Let us make an account of the notation introduced so far. Consider the following generic operator

$$\text{generic notation :} \qquad \mathcal{X}^n_{x,a}.$$

Then, the symbol $\mathcal{X} = \mathcal{Q}, \mathcal{P}, \mathcal{T}$ represents the information that the operator provides (flow rate, pressure or total pressure), index $x = q, p, t$ denotes the information that the operator receives (flow rate, pressure or total pressure), index $a = 1, 2$ indicates the vessel which the operator is related to, and index $n = 0, 1, 2, \ldots$ denotes the dependence of the operator in relation to the history of the state of the system.

Remark 2. In the case of complex networks (see Figure 2) a component may have multiple coupling interfaces. Since the choice of the boundary conditions remains arbitrary, such multiple-coupled component may receive as boundary information different quantities (flow rate in a subset of the coupling interfaces and pressure in the complementary subset). Therefore, a notation like the one introduced above is not identifiable.

3.3. Solvers for non-linear problems

Going back to our simplest example of Figure 1, we have seen how at time step n we arrive at the two-equation system

$$\mathcal{F}^n_1(Q^n, P^n) = 0, \tag{11}$$
$$\mathcal{F}^n_2(Q^n, P^n) = 0. \tag{12}$$

In particular, if at the coupling point C the boundary conditions chosen are flow rate for sub-network 1 and pressure for sub-network 2, these equations read

$$P^n - \mathcal{P}^n_{q,1}(Q^n) = 0, \tag{13}$$
$$Q^n - \mathcal{Q}^n_{p,2}(P^n) = 0. \tag{14}$$

It remains to select an iterative solver for this nonlinear system, maintaining the black-box structure of the strategy. Perhaps the easiest to implement is the Gauss-Seidel method, which reads

$$\begin{aligned} \mathcal{F}^n_1(Q^{n,k}, P^{n,k-1}) &= 0, \\ \mathcal{F}^n_2(Q^{n,k}, P^{n,k}) &= 0, \end{aligned}$$

where the iterations start at some initial guess $(Q^{n,0}, P^{n,0})$, usually taken as (Q^{n-1}, P^{n-1}) and stop at the iterate k for which both $|\mathcal{F}^n_1(Q^{n,k}, P^{n,k})|$ and $|\mathcal{F}^n_2(Q^{n,k}, P^{n,k})|$ are sufficiently small. For system (13)–(14) the Gauss-Seidel method thus reads

$$\begin{aligned} P^{n,k} &= \mathcal{P}^n_{q,1}(Q^{n,k-1}), \\ Q^{n,k} &= \mathcal{Q}^n_{p,2}(P^{n,k}). \end{aligned}$$

Notice that these iterations are nothing but the well-known Dirichlet-to-Neumann strategy, very popular in the domain decomposition literature. The sub-domains interact along the iterations in such a way that the pressure obtained at C from sub-network 1 is imposed as boundary condition to sub-network 2, while the flow rate obtained at C from sub-network 2 is imposed as boundary condition to sub-network 1. In the applications we consider this is not a clever choice, as will be illustrated in the examples. Instead, we propose to apply more sophisticated solvers for non-linear equations, focusing on an orthogonalized variant of Broyden's method and on the Newton-GMRES method [25, 26].

Let us recall these two methods, which must be given in matrix-free form. That is, we revisit the Broyden and Newton-GMRES applied to the particular system of equations (11)–(12). To do this consider that at time n, iteration $k-1$ the interface is not at equilibrium, therefore we can evaluate two residuals

$$\begin{aligned} R_1^{n,k-1} &= \mathcal{F}_1^n(Q^{n,k-1}, P^{n,k-1}), \\ R_2^{n,k-1} &= \mathcal{F}_2^n(Q^{n,k-1}, P^{n,k-1}). \end{aligned}$$

To reduce the notation we put

$$\begin{aligned} R^{n,k-1} &= (R_1^{n,k-1}, R_2^{n,k-1}), \\ X^{n,k-1} &= (Q^{n,k-1}, P^{n,k-1}), \\ \mathcal{F}^n(X^{n,k-1}) &= (\mathcal{F}_1^n(Q^{n,k-1}, P^{n,k-1}), \mathcal{F}_2^n(Q^{n,k-1}, P^{n,k-1})). \end{aligned}$$

Hence, the residual $R^{n,k-1}$ drives the state of the system $X^{n,k-1}$ from iteration $k-1$ to k.

We define the operator B^n which is an approximation of the Jacobian of the interface operator given by Broyden's algorithm at time t_n. In the orthogonalized version of Broyden's method the iterations evolve according to the following algorithm for a system of m non-linear equations: at time step n, given $X^{n,0} = X^{n-1}$ and given $\mathsf{B}^{n,0}$, compute $R^{n,0} = \mathcal{F}^n(X^{n,0})$ and do

1. For $j = 0$ to m
2. $\quad W^j = -(\mathsf{B}^{n,j})^{-1} R^{n,j}$
3. $\quad V = W^j$
4. $\quad$ For $i = 0$ to $j-1$
5. $\quad\quad V = V - (V, W^i)W^i$
6. $\quad$ Enddo
7. $\quad V = \frac{V}{\|V\|}$
8. $\quad X^{n,j+1} = X^{n,j} + V^j$
9. $\quad R^{n,j+1} = \mathcal{F}^n(X^{n,j+1})$

10. $\mathsf{B}^{n,j+1} = \mathsf{B}^{n,j} + \frac{R^{n,j+1} \otimes V}{(V, W^j)}$

11. Enddo

In the previous algorithm (U, V) and $U \otimes V$ denote the classical scalar and tensorial products between two vectors U and V. The initial condition denoted by X^0 is also given. When steps 4 to 7 are carried out, the algorithm is referred to as the *orthogonalized version* of Broyden's method. If these steps are skipped, we refer to it simply as Broyden's method.

Remark 3. When a time step, say n, converged at iteration k, an approximation of the Jacobian, denoted by $\mathsf{B}^{n,k}$, is available. This approximation is then employed to initialize the approximate Jacobian at step $n+1$, setting $\mathsf{B}^{n+1,0} = \mathsf{B}^{n,k}$. In this context Broyden's method with initialization resembles a preconditioned method, in contrast with the Newton-GMRES that just makes use of the previous state to initialize the iterations, without any preconditioning. In the numerical tests this has proven to be a remarkable advantage of Broyden's methods. In what concerns the choice of the first matrix, $\mathsf{B}^{0,0}$, in the cases treated here it has been considered as the identity matrix (case without initialization) or a finite difference estimation of the Jacobian matrix (case with initialization). For very long simulations, in which a large time step is used, it is advisable to perform a *restart* of the initialized algorithm erasing the last computed matrix B replacing it by a fresh finite difference approximation of the Jacobian.

For the Newton-GMRES algorithm the iterates are obtained as follows (for a system of m non-linear equations): at time step n, given $X^{n,0} = X^{n-1}$ and given σ, compute $R^{n,0} = \mathcal{F}^n(X^{n,0})$ and do

1. $V^1 = \frac{R^{n,0}}{\|R^{n,0}\|}$
2. For $j = 1$ to m
3. $\quad W^j = \frac{1}{\sigma}[\mathcal{F}^n(X^{n,0}) - \mathcal{F}^n(X^{n,0} + \sigma V^j)]$
4. $\quad$ For $i = 1$ to j
5. $\quad\quad H^{i,j} = (W^j, V^i)$
6. $\quad\quad W^j = W^j - H^{i,j} V^i$
7. $\quad$ Enddo
8. $\quad H^{j+1,j} = \|W^j\|$
9. $\quad V^{j+1} = \frac{W^j}{H^{j+1,j}}$
10. Enddo
11. $X^{n,m} = X^{n,0} + \mathsf{V}^m (\mathsf{H}^m)^{-1} \|R^{n,0}\| E^1$

In this algorithm V^m is formed by the vectors V, $H^{i,j}$ are the entries of the matrix H^m and E^1 is the canonical vector for the first component. Also, the initial condition, denoted by X^0, is given.

Remark 4. Any other solver for non-linear equations in matrix-free form can be used in the present framework.

In the previous descriptions of Broyden's and Newton-GMRES algorithms the stopping criterion is not detailed. In the actual implementation a (standard) stopping criterion is of course incorporated.

3.4. Computational implementation

The time discretization of the initial-boundary value problem (1)-(3) is carried out with a semi-implicit scheme. A Galerkin Least Squares formulation with upwinding along the characteristic lines is used for the spatial discretization. The discretization of the problem is briefly described for the pure elastic case ($K = 0$ in equation (3)) in what follows.

Consider the equations (1) and (2) of the 1D model recasted in the corresponding expressions along the characteristic lines

$$\frac{DQ}{Dt} - f^+ \frac{DA}{Dt} = g \qquad \text{along} \qquad \dot{x} = f^-(x(t), t), \tag{15}$$

$$\frac{DQ}{Dt} - f^- \frac{DA}{Dt} = g \qquad \text{along} \qquad \dot{x} = f^+(x(t), t), \tag{16}$$

with

$$g = -\frac{A}{\rho}\left(\frac{\partial P}{\partial \chi_i}\frac{\partial \chi_i}{\partial x} + f_r \frac{\rho |U| U}{4R}\right), \tag{17}$$

where χ_i are the material and geometrical parameters involved in the expression of P, while

$$f^{\pm} = \frac{Q}{A} \pm \sqrt{\frac{A}{\rho}\frac{\partial P}{\partial A}}. \tag{18}$$

Now we discretize in time both equations (15) and (16) as follows

$$\frac{Q^{n+1} - Q^n}{\Delta t} + f^- \left.\frac{\partial Q}{\partial x}\right|_{n+\theta} - f^+ \left(\frac{A^{n+1} - A^n}{\Delta t} + f^- \left.\frac{\partial A}{\partial x}\right|_{n+\theta}\right) = g^{n+\theta},$$

$$\frac{Q^{n+1} - Q^n}{\Delta t} + f^+ \left.\frac{\partial Q}{\partial x}\right|_{n+\theta} - f^- \left(\frac{A^{n+1} - A^n}{\Delta t} + f^+ \left.\frac{\partial A}{\partial x}\right|_{n+\theta}\right) = g^{n+\theta},$$

where $\frac{1}{2} \leq \theta \leq 1$. Then we introduce a finite element discretization of the 1D domain, denoted by I, with linear interpolation for the unknowns Q and A. Let $\mathcal{N}$ be the set of nodes of the finite element mesh for I, then the computation of

the two residuals reads

$$R_i^{\pm} = \frac{Q_i^{n+1}\phi_i - Q_i^n\phi_i}{\Delta t} + f^{\pm}\left.\frac{\partial \phi_i}{\partial x} Q_i\right|_{n+\theta} - f^{\mp}\left(\frac{A_i^{n+1}\phi_i - A_i^n\phi_i}{\Delta t} + f^{\pm}\left.\frac{\partial \phi_i}{\partial x} A_i\right|_{n+\theta}\right) - g^{n+\theta} \qquad i \in \mathcal{N}.$$

Finally, the set of equations is attained through a least squares technique, yielding

$$\int_I (R_i^- \mathcal{L}_{Q,j}^- + R_i^+ \mathcal{L}_{Q,j}^+)\,\mathrm{d}x = 0 \qquad \forall \phi_j,\ j \in \mathcal{N}, \tag{19}$$

$$\int_I (R_i^- \mathcal{L}_{A,j}^- + R_i^+ \mathcal{L}_{A,j}^+)\,\mathrm{d}x = 0 \qquad \forall \phi_j,\ j \in \mathcal{N}, \tag{20}$$

where the upwinding is taken into account within the weighting functions

$$\mathcal{L}_{Q,j}^{\mp} = \phi_j + f^{\mp}\tau^{\mp}\frac{\partial \phi_j}{\partial x}, \qquad j \in \mathcal{N}, \tag{21}$$

$$\mathcal{L}_{A,j}^{\mp} = f^{\pm}\left(\phi_j + f^{\mp}\tau^{\mp}\frac{\partial \phi_j}{\partial x}\right) \qquad j \in \mathcal{N}. \tag{22}$$

Here $\tau^{\mp}$ are the characteristic times that play the role of the stabilization parameters, which are chosen as follows

$$\tau^{\mp} = \frac{\Delta x}{2|f^{\mp}|}. \tag{23}$$

Finally, the third equation, see (3), is a node-wise pressure-area relation in the case of a pure elastic model.

The scheme is run with $\theta = 0.5$, and all the non-linearities in the problem are treated with Picard iterations. This fixed point approach implies evaluating the quantities in equations (17), (18), (21), (22) and (23) at the previous iteration. Particularly, the characteristics $f^{\pm}$ are computed at $t^{n+\theta}$ and are evaluated element-wise, taking the mean value given by the contribution of the quantities in the two nodes of the linear elements.

In case of bifurcations the conservation of flow rate and continuity of pressure are enforced. For the implementation of the terminal elements and the heart inflow boundary condition the reader is referred to [27] for further details.

For the viscoelastic model we split the pressure in (3) into two contributions the elastic pressure P_e (first two terms in the right hand side of (3)) and the viscoelastic counterpart P_v (last term in the right hand side of (3)). We add one unknown for implementation issues, that is P_e, which is treated in the same manner as in the pure elastic model. The viscoelastic part, which is a function of $\frac{\partial A}{\partial t}$ is introduced in the equations using the mass equation. Thus the system is written in terms of the unknowns (Q, A, P_e, P), where $P = P_e + P_v$. The interested reader is referred to [28, 29] for more details.

3.5. Inner and outer iterations

In this kind of problems we have two levels of non-linearity. The inner level refers to the iterations performed to assess the residual in the solution process (step 9 in Broyden and step 3 in Newton-GMRES). At this level the non-linear problem is solved by carrying out inner iterations, that is, iterations of the black-box solver corresponding to each individual sub-network. In turn, the outer level refers to the iterations of the solver (Broyden, Newton-GMRES, etc.) of the non-linear interface problem.

In some cases, the inner iterations can be eliminated (i.e., limited to just one) to reduce computational cost. Some results will be presented so as to assess how the removal of inner iterations affects the convergence of the outer iterations.

For our specific sub-network solver each inner iteration corresponds to solving (19)-(20) with (18) frozen at its last computed value, so that the system for Q and A becomes linear and is solved by Gauss elimination. This is a simple fixed-point strategy that could obviously be improved, but notice that this would correspond to improving the black boxes that deal with each sub-network and is thus not the point of this article. Indeed, a worst-case-scenario type of reasoning suggests that, to assess the reliability of our coupling methodology, the black boxes used for the sub-networks should be kept as simple as possible.

4. Numerical tests

In this section two academic examples are presented. They aim at studying the performance of the iterative coupling algorithm based on Broyden's method in terms of reliability, not focusing in its convenience in terms of computing time with respect to a monolithic approach since such comparisons would obviously depend on the size of problem. For a given partition of the network, however, the cost is roughly proportional to the number of inner iterations, which allows for meaningful comparisons among the several possible variants of our algorithm.

The units used in this section are: cm for length, sec for time, and dyn/cm^2 for pressure.

4.1. 1D-1D pipe decomposition

In this example a pipe is split into two identical pipes, and a flow rate wave is imposed such that it travels from left to right across the domain. Figure 3 shows the pipe, the boundary condition at the leftmost point and some dimensions. The parameters that define the problem are $L = 300$, $R_0 = 1$, $h = 0.1$, $E = 200000$, $K = 0$, $\rho = 1$, $\mu = 0$ (the viscosity for the friction factor f_r) and $P_0 = 0$, whereas the spatial discretization is given by $\Delta x = 0.2$. For the time integration two time steps are used $\Delta t_1 = 0.0005$ and $\Delta t_2 = 0.005$. With these data the wave speed is $c = \sqrt{\frac{Eh}{2\rho R_0}} = 100$ according to the Moens-Korteweg approximation. The flow rate boundary condition is imposed and is of the form $Q_{bc}(t) = Q_0(1 - \cos(2\pi t/T))$, with $Q_0 = 2.5$ and $T = 0.36$ for which the wavelength resulted $\lambda_1 = 36$. Although it is not relevant here, because the wave does not reach the outflow boundary, on the rightmost point a reflecting

boundary is considered, which is a large value of the terminal impedance when compared with the impedance of the 1D segment.

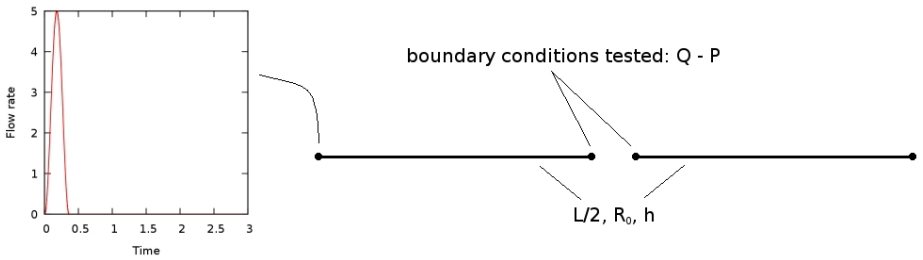

Figure 3: Decomposition of a pipe into two vessels.

In the first part of the example the partitioned approach referred to in the following corresponds to the imposition of pressure at both sides of the coupling point, which means the system of non-linear equations is of the form

$$Q^n = \mathcal{Q}^n_{p,1}(P^n),$$
$$Q^n = \mathcal{Q}^n_{p,2}(P^n).$$

In this first analysis we employ Broyden's method as the iterative solver. The results obtained with the monolithic 1D segment are also presented and we compare also the sensitivity to the presence of inner iterations and to the time step.

Figure 4 shows the wave propagating throughout the domain for the case $\Delta t_1 = 0.0005$. The differences in the results obtained with monolithic and partitioned approaches are negligible, as expected (since at all time steps the interface system of equations converged). The converged results are also independent on whether the inner iterations are allowed to converged or are limited to one.

For the case $\Delta t_1 = 0.0005$, Figure 5 displays a comparison of the performance of orthogonalized Broyden's method with and without inner iterations. Observe that the iterations increase when the wave traverses the coupling point. When the inner iterations are allowed to converge, the outer iterations are significantly reduced. Nevertheless, since the number of inner iterations to bring the residual to zero (within tolerance) ranged between 2 and 3, it turns out to be convenient to solve the problem without performing inner iterations. Inner iterations are only necessary in the case of larger time steps, or in the case of more complex sub-networks. In such cases, the absence of inner iterations led to diverging iterative schemes, as will be shown in forthcoming sections.

Turning now to the convergence of the iterative solver when increasing the time step from $\Delta t_1 = 0.0005$ to $\Delta t_2 = 0.005$, without inner iterations, Figure 6 shows that the increase in the time step does not significantly affect the number of iterations needed at each time step. Nevertheless, one or two more iterations are needed after the wave crosses the interface, which appears to arise from a

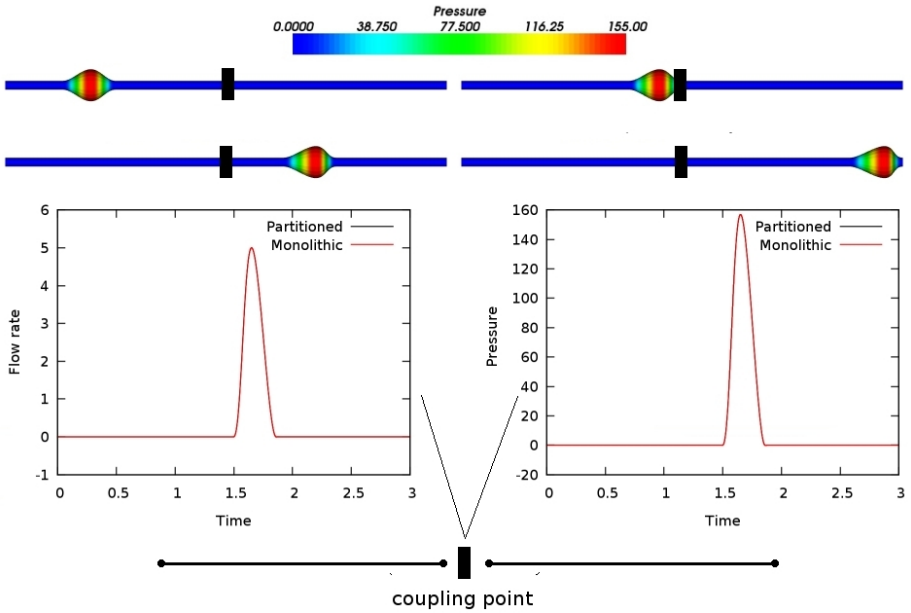

Figure 4: Comparison between monolithic and partitioned approaches (simulation data: orthogonalized Broyden's method, $\Delta t = 0.0005$, pressure boundary conditions everywhere).

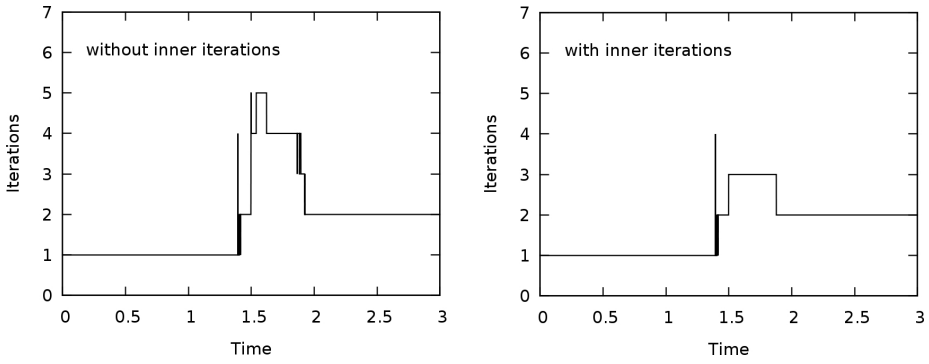

Figure 5: Performance of the iterative strategy with and without inner iterations (simulation data: simple pipe case, orthogonalized Broyden's method, $\Delta t = 0.0005$, pressure boundary conditions everywhere).

numerical difficulty in dealing with the wake of the wave. This is related to the time advancing scheme employed here. In spite of this, notice that a tenfold increase in the time step changed the number of iterations only slightly. Large time steps may require inner iterations to achieve convergence, as will be seen in the hemodynamics regime.

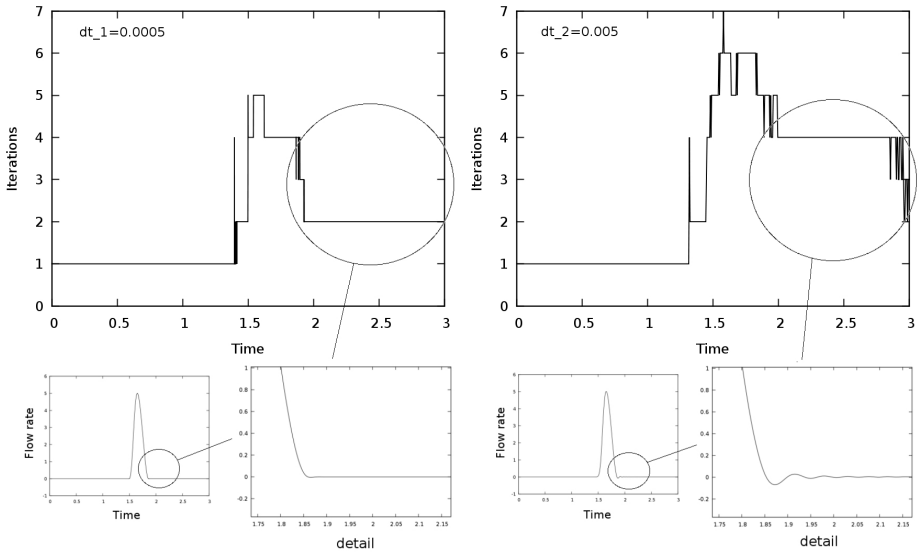

Figure 6: Performance of the iterative strategy for time steps $\Delta t_1 = 0.0005$ and $\Delta t_2 = 0.005$ (simulation data: simple pipe case, orthogonalized Broyden's method, pressure boundary conditions everywhere, without inner iterations).

The last numerical experiment in this example is concerned with a modification in the setting of boundary conditions at the coupling point for both partitions. A pressure–pressure, denoted now by P–P, boundary condition has been analyzed so far. Now we will study other combinations, namely Q–Q, Q–P and P–Q boundary conditions. Here inner iterations are not performed and the time step is fixed at $\Delta t_1 = 0.0005$. In Figure 7 the four combinations are drawn. The results are not conclusive, in the sense that no clear advantage of some of the tested boundary conditions is apparent.

Finally, we compared in Figure 8 the performance of Broyden's method with and without orthogonalization. The number of iterations is clearly reduced when performing the orthogonalization procedure. In some tested cases, this orthogonalization procedure may bring numerical instabilities to the iterative algorithm. In such situations, Broyden's method without orthogonalization results in a more stable solver. However, whenever possible, it is recommended to use the orthogonalized version of Broyden's method.

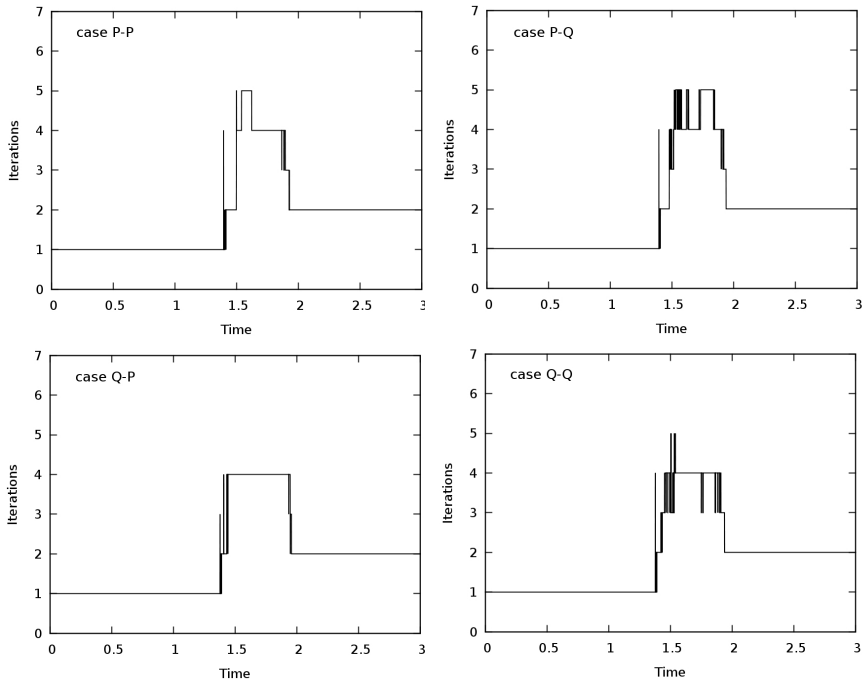

Figure 7: Iterations for different boundary conditions imposed (simulation data: simple pipe case, orthogonalized Broyden's method, $\Delta t = 0.0005$, without inner iterations).

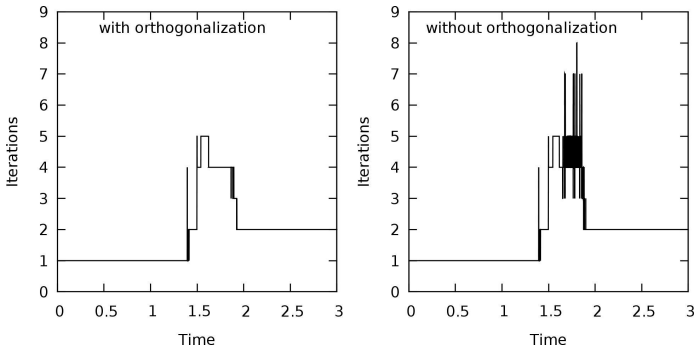

Figure 8: Performance of Broyden's method with and without orthogonalization (simulation data: simple pipe case, $\Delta t = 0.0005$, without inner iterations).

4.2. Tree-like structure

Consider the network shown in Figure 9, which is set up as follows. The flow rate boundary condition of the previous example is imposed at the root of the tree. All the terminal points (outflow boundaries) are reflecting ones (a large value of the terminal impedance when compared with the impedance of the 1D segments, in this case such impedance is 10^8). The geometrical characteristics at the root (level 0) are $L = 20$, $R_0 = 1$, $h = 0.1R_0$, $E_0 = 200000$, $K = 0$, $\rho = 1$, $\mu = 0$ (the viscosity for the friction factor f_r) and $P_0 = 0$. At the other levels the lengths of the segments are maintained (equal to L), and the following alteration of the properties is considered: $E_i = E_0 + i\Delta E$, $\Delta E = 50000$, $R_i = (1 - i/10)R_0$, $i = 1, 2, 3, 4$. The spatial discretization is defined by $\Delta x = 0.1$ and the time integration ranges from $\Delta t = 0.00025$ to $\Delta t = 0.025$. The tree is set up that way so as to establish a somewhat similar structural topology concerning geometrical and material behavior to the one encountered in the arterial tree, although it is not strictly within the physiological regime.

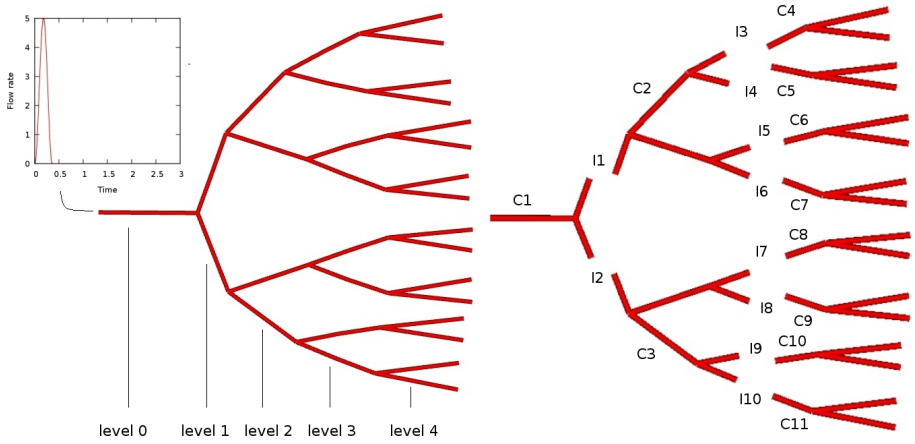

Figure 9: Network structure, level-based decomposition and resulting sub-networks.

The decomposition of the network into sub-networks is done following a level-based criterion as shown also in Figure 9 with an identification of the ten coupling interfaces. The network is composed by five levels of vessels, from the root to the leaves and the system is split into 11 sub-networks as seen in the afore referred figure. The partitioned system is decomposed such that sub-networks with different number of coupling points arise. For completeness purposes we present the whole set of interface equations in the case of imposing pressure boundary conditions everywhere. The (twenty) equations are ordered according

to the interface to which they correspond, yielding

$$
\begin{aligned}
\mathcal{F}^n_{I1,1}(\mathbf{Q}^n,\mathbf{P}^n) &= Q^n_{I1} - \mathcal{Q}^n_{p,I1,C1}(P^n_{I1},P^n_{I2}),\\
\mathcal{F}^n_{I1,2}(\mathbf{Q}^n,\mathbf{P}^n) &= Q^n_{I1} - \mathcal{Q}^n_{p,I1,C2}(P^n_{I1},P^n_{I3},P^n_{I4},P^n_{I5},P^n_{I6}),\\
\mathcal{F}^n_{I2,1}(\mathbf{Q}^n,\mathbf{P}^n) &= Q^n_{I2} - \mathcal{Q}^n_{p,I2,C1}(P^n_{I1},P^n_{I2}),\\
\mathcal{F}^n_{I2,2}(\mathbf{Q}^n,\mathbf{P}^n) &= Q^n_{I2} - \mathcal{Q}^n_{p,I2,C3}(P^n_{I2},P^n_{I7},P^n_{I8},P^n_{I9},P^n_{I10}),\\
\mathcal{F}^n_{I3,1}(\mathbf{Q}^n,\mathbf{P}^n) &= Q^n_{I3} - \mathcal{Q}^n_{p,I3,C2}(P^n_{I1},P^n_{I3},P^n_{I4},P^n_{I5},P^n_{I6}),\\
\mathcal{F}^n_{I3,2}(\mathbf{Q}^n,\mathbf{P}^n) &= Q^n_{I3} - \mathcal{Q}^n_{p,I3,C4}(P^n_{I3}),\\
\mathcal{F}^n_{I4,1}(\mathbf{Q}^n,\mathbf{P}^n) &= Q^n_{I4} - \mathcal{Q}^n_{p,I4,C2}(P^n_{I1},P^n_{I3},P^n_{I4},P^n_{I5},P^n_{I6}),\\
\mathcal{F}^n_{I4,2}(\mathbf{Q}^n,\mathbf{P}^n) &= Q^n_{I4} - \mathcal{Q}^n_{p,I4,C5}(P^n_{I4}),\\
\mathcal{F}^n_{I5,1}(\mathbf{Q}^n,\mathbf{P}^n) &= Q^n_{I5} - \mathcal{Q}^n_{p,I5,C2}(P^n_{I1},P^n_{I3},P^n_{I4},P^n_{I5},P^n_{I6}),\\
\mathcal{F}^n_{I5,2}(\mathbf{Q}^n,\mathbf{P}^n) &= Q^n_{I5} - \mathcal{Q}^n_{p,I5,C6}(P^n_{I5}),\\
\mathcal{F}^n_{I6,1}(\mathbf{Q}^n,\mathbf{P}^n) &= Q^n_{I6} - \mathcal{Q}^n_{p,I6,C2}(P^n_{I1},P^n_{I3},P^n_{I4},P^n_{I5},P^n_{I6}),\\
\mathcal{F}^n_{I6,2}(\mathbf{Q}^n,\mathbf{P}^n) &= Q^n_{I6} - \mathcal{Q}^n_{p,I6,C7}(P^n_{I6}),\\
\mathcal{F}^n_{I7,1}(\mathbf{Q}^n,\mathbf{P}^n) &= Q^n_{I7} - \mathcal{Q}^n_{p,I7,C3}(P^n_{I2},P^n_{I7},P^n_{I8},P^n_{I9},P^n_{I10}),\\
\mathcal{F}^n_{I7,2}(\mathbf{Q}^n,\mathbf{P}^n) &= Q^n_{I7} - \mathcal{Q}^n_{p,I7,C8}(P^n_{I7}),\\
\mathcal{F}^n_{I8,1}(\mathbf{Q}^n,\mathbf{P}^n) &= Q^n_{I8} - \mathcal{Q}^n_{p,I8,C3}(P^n_{I2},P^n_{I7},P^n_{I8},P^n_{I9},P^n_{I10}),\\
\mathcal{F}^n_{I8,2}(\mathbf{Q}^n,\mathbf{P}^n) &= Q^n_{I8} - \mathcal{Q}^n_{p,I8,C9}(P^n_{I8}),\\
\mathcal{F}^n_{I9,1}(\mathbf{Q}^n,\mathbf{P}^n) &= Q^n_{I9} - \mathcal{Q}^n_{p,I9,C3}(P^n_{I2},P^n_{I7},P^n_{I8},P^n_{I9},P^n_{I10}),\\
\mathcal{F}^n_{I9,2}(\mathbf{Q}^n,\mathbf{P}^n) &= Q^n_{I9} - \mathcal{Q}^n_{p,I9,C10}(P^n_{I9}),\\
\mathcal{F}^n_{I10,1}(\mathbf{Q}^n,\mathbf{P}^n) &= Q^n_{I10} - \mathcal{Q}^n_{p,I10,C3}(P^n_{I2},P^n_{I7},P^n_{I8},P^n_{I9},P^n_{I10}),\\
\mathcal{F}^n_{I10,2}(\mathbf{Q}^n,\mathbf{P}^n) &= Q^n_{I10} - \mathcal{Q}^n_{p,I10,C11}(P^n_{I10}),
\end{aligned}
$$

where $\mathbf{Q}^n = (Q^n_{I1},\ldots,Q^n_{I10})$ and $\mathbf{P}^n = (P^n_{I1},\ldots,P^n_{I10})$.

The results obtained with the partitioned structure using Broyden's algorithm, for $\Delta t = 0.0025$, are shown in Figure 10, and coincide with those obtained with the monolithic system. In this case the presence of reflections determines a far more complex pattern of forward and backward travelling waves, imposing the need for more advanced iterative algorithms. These results correspond to imposing pressure boundary information to all sub-networks at each coupling interface.

We first compare the performance as a function of the time step Δt. In Figure 11 the number of iterations throughout the simulation for $\Delta t_1 = 0.00025$, $\Delta t_2 = 0.0025$ and $\Delta t_3 = 0.025$ is shown, when the inner iterations are performed until convergence. In this example, convergence of the inner iterations for the larger time steps, $\Delta t = 0.0025$ and $\Delta t = 0.025$, is necessary for the algorithm not to diverge. On the other hand, for $\Delta t = 0.00025$ the number of iterations at each time step is almost insensitive to the existence or not of inner iterations.

A last test is carried out in this example. Remember that all the results so far in this section were obtained imposing a pressure boundary condition

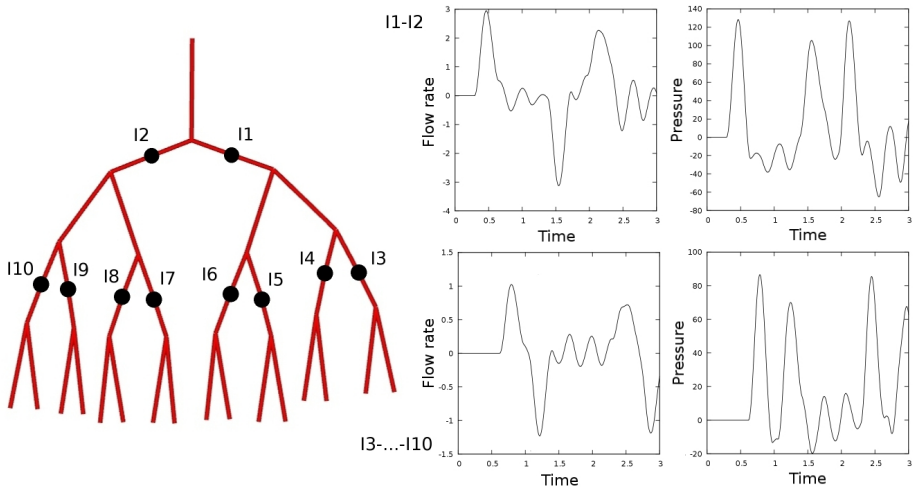

Figure 10: Results at coupling interfaces (simulation data: Broyden's method, $\Delta t = 0.0025$, pressure boundary conditions everywhere).

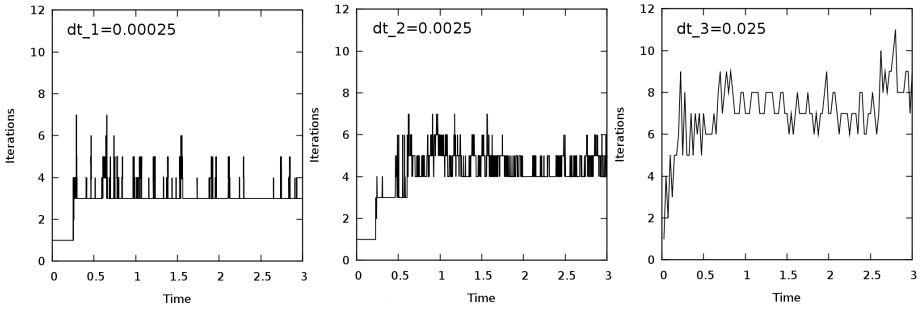

Figure 11: Iterations until convergence for different time steps (simulation data: tree-like case, Broyden's method, pressure boundary conditions everywhere, with inner iterations).

at both sides of each coupling points (at the two arriving sub-networks). Now we change this to a flow rate boundary condition. In Figure 12 the results are presented. From the larger number of iterations, we conclude that the case with flow rate boundary conditions corresponds to a worse conditioned system of non-linear equations. This case was set up allowing for inner iterations and with $\Delta t = 0.0025$. Further increase of the time step -of the order of $\Delta t = 0.025$- combined with a flow rate boundary condition did not result in convergent iterative schemes.

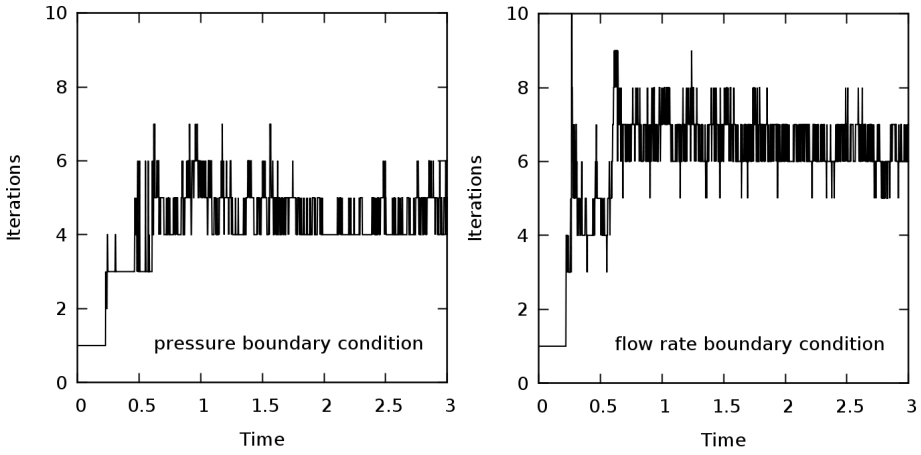

Figure 12: Comparison between pressure and flow rate boundary conditions (simulation data: tree-like case, Broyden's method, $\Delta t = 0.0025$, with inner iterations).

5. Application in hemodynamics

This section is devoted to the application of the iterative strategies developed in the previous sections to specific situations found in the modeling of the cardiovascular system.

5.1. Vasculature network

Consider the 1D network shown in Figure 13, containing 150 vessels and based on the arterial tree presented in [2]. The material and geometrical parameters are also set according to [2], and a viscoelastic model (not provided for brevity) is adopted for the arterial wall. The outflow boundary conditions are given by means of 0D Windkessel models calibrated to meet the main characteristics of the vascular tree: flow distribution and equivalent compliances of the different components of the system. The calibration of the 0D lumped models is carried out based on the guidelines and data given in [15, 30]. The inflow boundary condition at the heart was taken from [31] and re-scaled so as to have mean flow rate $Q = 5.6$ lt/min and period $T = 1.2$ sec (see also Figure 13). This regime implies that the system is at-rest, with 50 beats per minute. Though

some details have been skipped for brevity, this network allows for an assessment of the proposed methodology on an extensive systemic network.

5.2. Hierarchical decomposition

The whole arterial system is decomposed into 7 sub-networks as shown in Figure 13. The decomposition follows a hierarchical approach in order to divide the systemic circulation into the 6 larger sub-systems corresponding to the main levels of circulation in the arterial network. Namely, the circulation through: the Aorta artery, both Subclavian arteries, both Carotid arteries and both Iliac arteries.

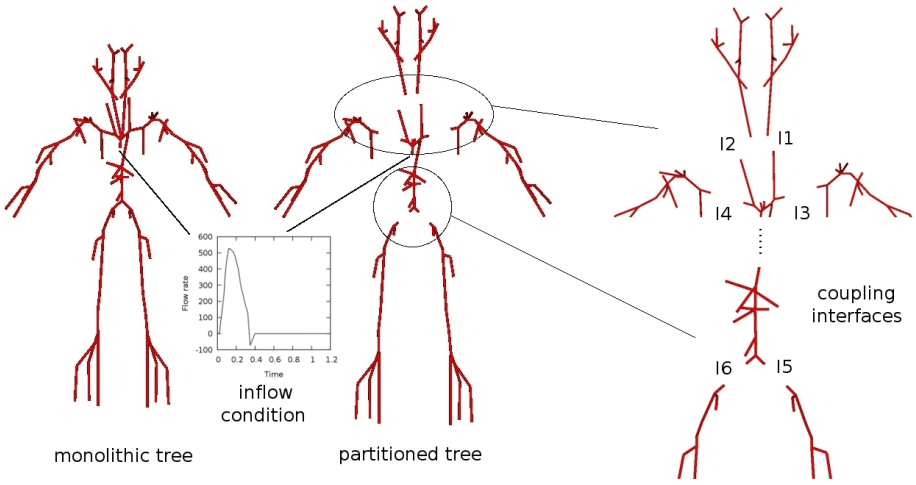

Figure 13: Arterial tree and hierarchical decomposition.

In Table 1 the number of degrees of freedom for each component after performing the discretization is detailed. Recall that the condition number in this kind of problems depends on the number of interface unknowns, and as said above the interface problem just consists of 12 unknowns. As a consequence, it is evident that, although we increase the number of unknowns in each component, the number of iterations to reach the convergence is almost insensitive to the refinement of the spatial discretizations of the sub-networks.

5.3. Numerical simulation

Here we focus on the comparison of different options for the situation corresponding to the at-rest regime as commented above. Concerning the comparison between the partitioned and the monolithic approaches, all the alternative iterative methods proposed here lead to the same solution up to the precision given by the convergence of the non-linear iterations among sub-systems (outer iterations). Figure 14 presents the results, flow rate and pressure, of the iterative (Newton-GMRES method in that figure) strategy for the six coupling points. These results correspond to pressure boundary conditions at all coupling points

Sub-component	Degrees of freedom
Aorta	999
Right carotid	576
Left carotid	570
Right subclavian	1179
Left subclavian	1215
Right iliac	1143
Left carotid	1140
Interface problem	12

Table 1: Discretization of each component of the arterial network.

for all the sub-systems and to a time step $\Delta t = 0.0025$, which is a reasonable value for implicit methods in computational hemodynamics.

Remark 5. All the computations performed here were obtained taking into account inner iterations to evaluate the residuals in each vasculature sub-network. Without inner iterations, as in the example treated in Section 4.2, the non-linear solvers did not converge. In the present case, even with $\Delta t = 0.000025$, it was not possible to avoid the inner iterations in the computations.

Three cardiac cycles were simulated, and just the results of the last period are plotted in Figure 14. Since the differences with the solution obtained with the monolithic approach are negligible, these are not displayed. Notice from the figure that each sub-network has a quite complex response. The main differences in the solution can be appreciated at each pair of coupling points. This is the result of the traveling and reflection of waves throughout the tree. Despite this, the partitioned approach performs quite well for the flow regimes encountered in hemodynamics as will be seen next.

Figure 15 compares the number of iterations used by Broyden's method (with initialization) with those of Newton-GMRES for the three cardiac cycles simulated. The lack of preconditioning in Newton-GMRES leads to a larger number of iterations until convergence. For Broyden's method note the higher number of iterations during the three systolic phases. In turn, Figure 16 shows a comparison between the iterations performed by Broyden's method for different combinations of boundary conditions, namely: (i) pressure everywhere, (ii) flow rate everywhere, (iii) flow rate to the aorta and pressure on the remaining part of the tree and (iv) pressure to the aorta and flow rate on the remaining part of the tree. The last two options are two representative cases of mixed boundary conditions. Other combinations were tested, and the results were qualitative and quantitative equivalent. We observe that the best performance is obtained when setting pressure boundary conditions everywhere.

With the previous numerical evidences we can conclude that for the cardiovascular regimes the best combination *solver–boundary condition* is Broyden's method with pressure boundary conditions for all the coupling points.

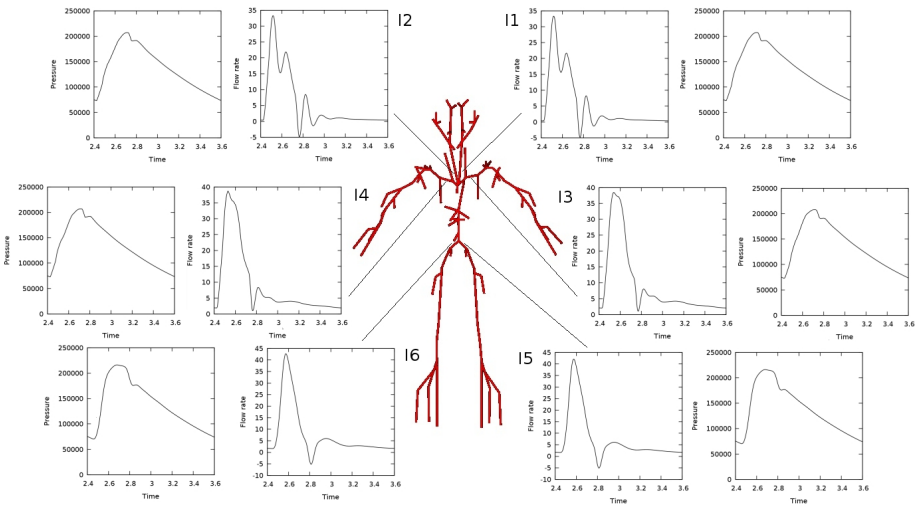

Figure 14: Results at coupling interfaces given by the partitioned approach (simulation data: Broyden's method, $\Delta t = 0.0025$, pressure boundary conditions everywhere, with inner iterations).

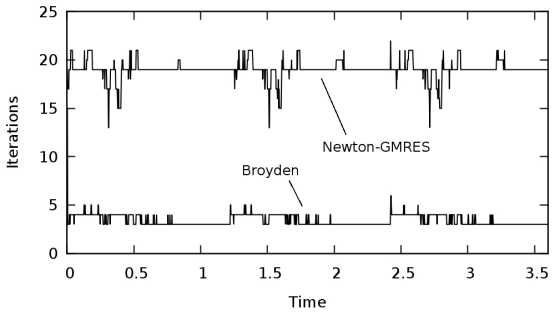

Figure 15: Iterations until convergence Broyden's and Newton-GMRES methods (simulation data: arterial network case, $\Delta t = 0.0025$, pressure boundary conditions everywhere, with inner iterations).

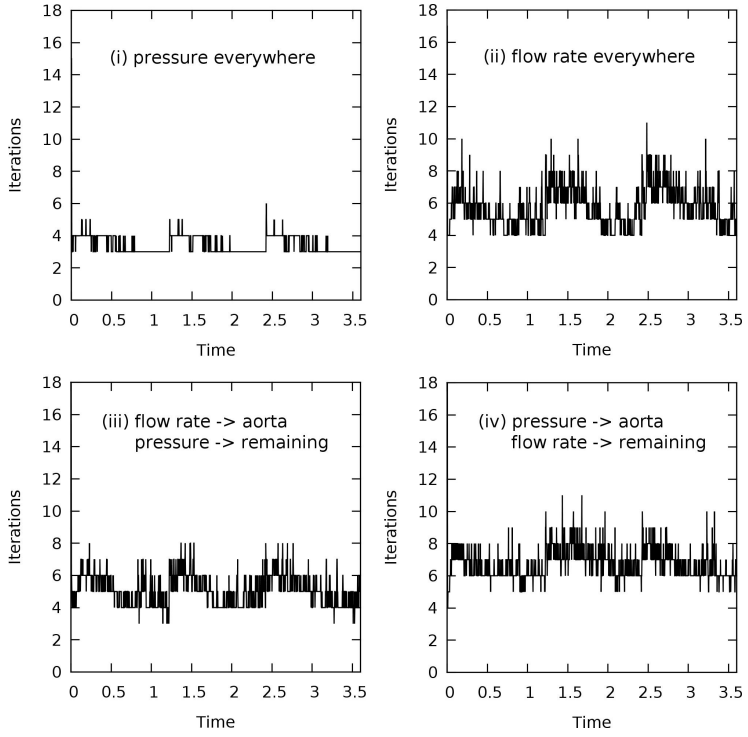

Figure 16: Comparison for different boundary conditions imposed throughout the three cardiac beats (simulation data: arterial network case, Broyden's method, $\Delta t = 0.0025$, with inner iterations).

Remark 6. In this case, the initialization of the matrix B in Broyden's method through the computation of the Jacobian, as commented in Remark 3, is mandatory for achieving convergence.

The use of a larger time step in Broyden's method ($\Delta t = 0.005$) required, for the cases analyzed here, a restart operation (see Remark 3) at the begining of each cardiac cycle in order to get convergence. Also notice in Figure 17 that the Newton-GMRES method converges even for larger time steps ($\Delta t = 0.005$ and $\Delta t = 0.01$). These results are obtained when the sub-networks at each coupling point receive pressure boundary conditions.

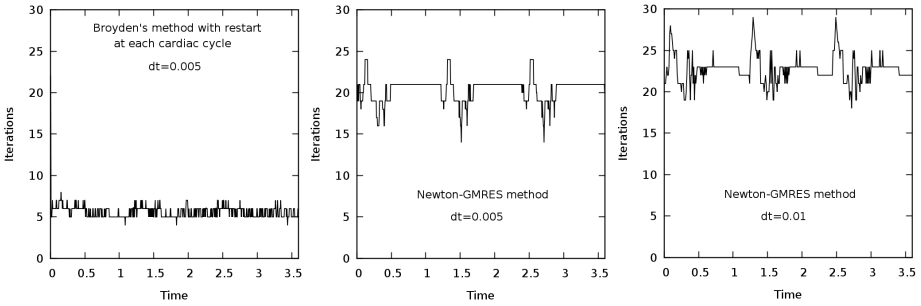

Figure 17: Broyden with restart of matrix B at each cardiac cycle and Newton-GMRES for larger time steps (simulation data: arterial network case, pressure boundary condition everywhere, with inner iterations).

For the sake of completeness we also tested the Gauss-Seidel method in this problem. In the case analyzed, flow rate boundary conditions were imposed at the aorta component, while the rest of the components received the pressure as boundary conditions. This is a particular example in which we combine flow rate and pressure boundary conditions. The time step used in the simulations was $\Delta t = 0.0025$.

In Figure 18 we plot the number of iterations needed by the Gauss-Seidel method with relaxation to converge for several relaxation parameters from which the optimal value can be inferred ($0.6 < \varsigma < 0.7$). The performance of Broyden's method in the same problem is clearly superior, as shown in the figure for comparison purposes. Also, for ς close to 1, the Gauss-Seidel method presents a much higher sensitivity with respect to the state of the heart ejection (contraction or expansion) than Broyden's and Newton-GMRES methods.

6. Further comments

The iterative strategy presented in the previous sections accounts for the partitioned -parallel- approach (except for the Gauss-Seidel method seen in the last case of analysis in Section 5). In this sense, at each iteration it was seen that it is possible to advance in time the different components in a completely separated fashion. Consequently, we can think of the following alternatives that go beyond the results featured in the present work

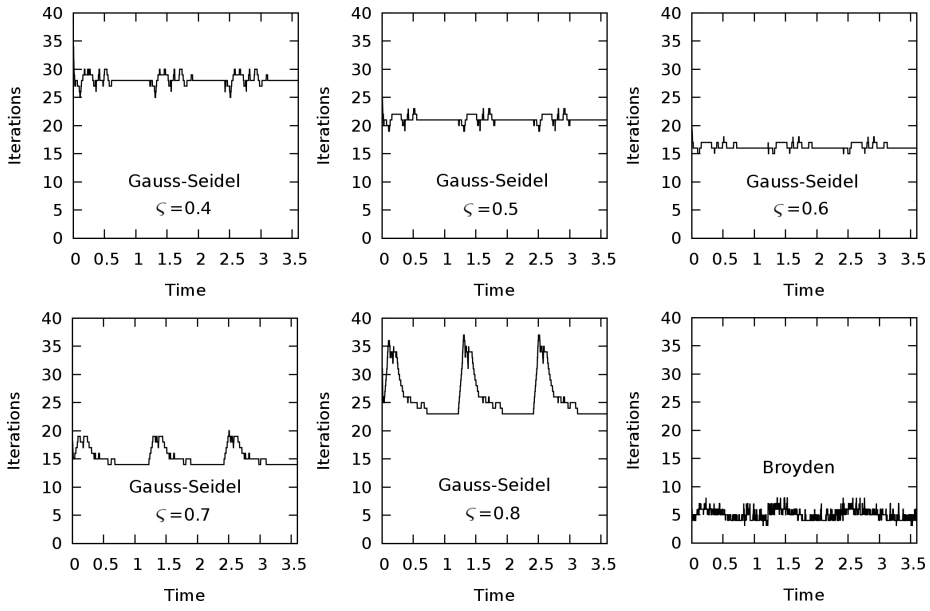

Figure 18: Gauss-Seidel with relaxation and Broyden's methods (simulation data: arterial network case, flow rate boundary conditions for the aorta and pressure boundary condition for the rest of the components, with inner iterations).

(i) setting different time marching schemes for the different components in the system;

(ii) setting different time steps (if we consider the same time marching scheme for all the sub-components);

(iii) setting different levels of time stepping (internal and external time-stepping).

Let us clarify the points (ii) and (iii) raised above with the example analyzed in Section 4.1. Let us consider the simple case of a vessel divided into two sub-networks for which we prescribe pressure boundary conditions at both sides of the coupling point.

6.1. Setting different time steps for different sub-networks

Two different time steps will be considered Δt_L and Δt_R for the left and right sub-networks, respectively. Two possibilities are tested: $\Delta t_L > \Delta t_R$ and $\Delta t_L < \Delta t_R$, that is for $M \in \mathbb{N}$, $\Delta t_L = M\Delta t_R$ and $\Delta t_R = M\Delta t_L$. In this case we can identify one global time discretization ($\max\{\Delta t_L, \Delta t_R\}$), which is the time step, owned by one of the sub-networks, used to interchange information among them, and one local time discretization ($\min\{\Delta t_L, \Delta t_R\}$) which is the time step that the other sub-network will use to advance form $n-1$ to n. Therefore, for instance, if we take $\Delta t_R = M\Delta t_L$ the procedure at one single iteration is the

following: given $P^{n,k}$ the right sub-network computes $\mathcal{Q}^n_{p,2}(P^{n,k})$ by performing one single time step given by Δt_R, whereas the left sub-network computes $\mathcal{Q}^n_{p,1}(P^{n,k})$ by marching along M time steps of length Δt_L. So, both components communicate with each other through the outer iterations, updating the values of the boundary conditions, according to the outer iterations which are ruled by operators discretized in time with Δt_R. For the example we analyze both cases of heterogeneous time stepping: (i) $\Delta t_L = 0.005$, $\Delta t_R = 0.0005$ and (ii) $\Delta t_L = 0.0005$ and $\Delta t_R = 0.005$, as compared to the standard case (iii), in which $\Delta t_L = \Delta t_R = \Delta t = 0.005$.

Figure 19 shows the comparison of the iterations and flow rate among these three situations. Observe that the number of iterations diminishes slightly when we reduce the time step in one of the two components. As well, we observe that the solution is almost the same, but for the differences appearing as a result of the specific time-stepping used for the different sub-networks.

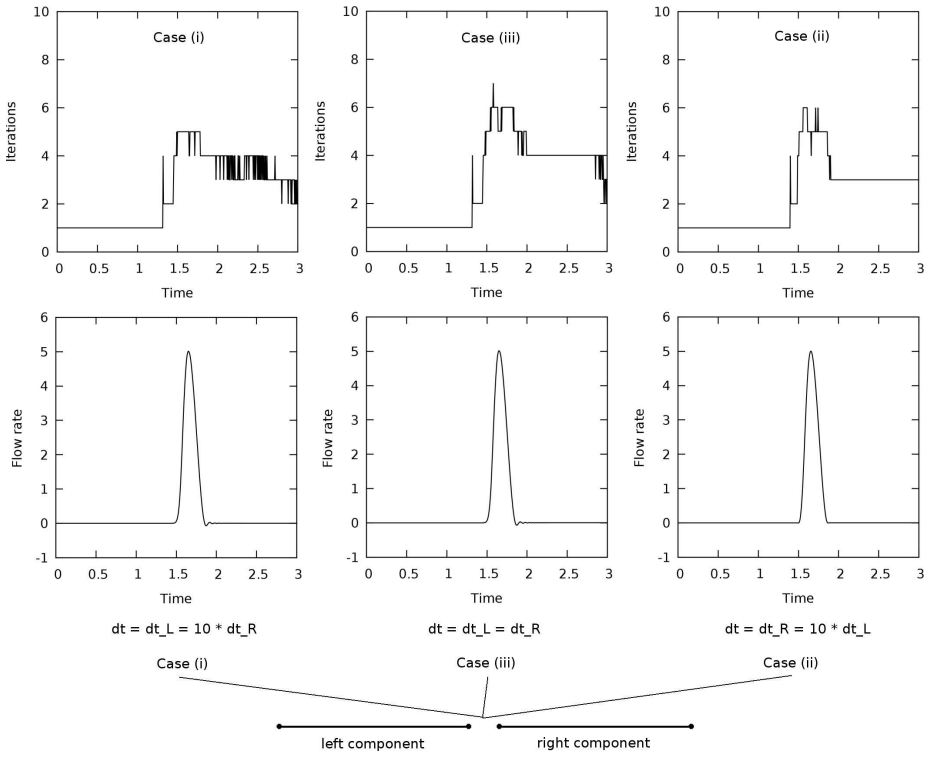

Figure 19: Solution at the coupling point. Comparison between the standard case (case (iii)) with cases using different time steps for the left and right sub-networks (simulation data: Broyden's method, $\Delta t = 0.005$, pressure boundary conditions everywhere, without inner iterations).

When we look at the solution in the left sub-network, say the middle point (see Figure 20), we note that some spurious reflections arise at the coupling

interface when we employ heterogeneous time stepping. These reflections are not present in the case with homogeneous time-step, that is case (iii), while they are more evident, about 2% of the incoming flow rate wave, in the case (ii). Such reflections are due to a difference in the stiffnesses of the sub-networks. As displayed in the details of the plots in Figure 20, when $\Delta t_L > \Delta t_R$ (case (i)) the right sub-network is stiffer than the left one and then a negative flow rate spurious wave appears travelling backwards. Contrariwise, when $\Delta t_R > \Delta t_L$ (case (ii)) the left sub-network is stiffer than the right one, and a positive spurious wave takes place.

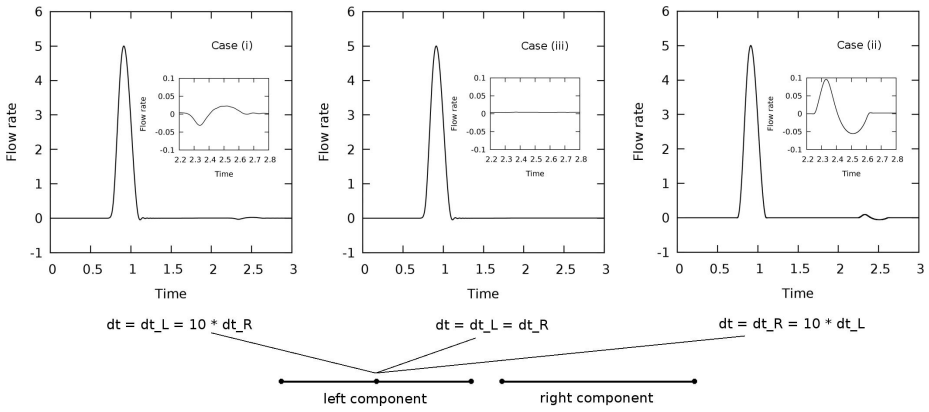

Figure 20: Spurious reflections travelling backwards in the left sub-network and comparison of solutions at the middle point of the left sub-network (simulation data: Broyden's method, $\Delta t = 0.005$, pressure boundary conditions everywhere, without inner iterations).

6.2. Setting different levels of time-stepping

Another issue that turns out to be interesting when using this independent time-marching schemes is that of performing communications not at every time step, but at a certain number of time steps. For instance, we can have that the time step used to advance the sub-networks from $n-1$ to n is Δt_I (an internal time step), while the time step at which the residuals are evaluated, in the Broyden's method, is $\Delta t_E \gg \Delta t_I$ (an external time step). This proves to be another capability of the decomposition strategy, motivated by the fact that the internal time step may be restricted by numerical instabilities intrinsic to the discretization method employed inside each black box, whereas the external time step is such that it ensures convergence of the coupling iterative algorithm.

We tested this internal/external time-marching scheme for the simple case studied in the previous section. The time steps used in the numerical tests are $\Delta t_I = 0.0005$ and $\Delta t_E = 0.005$. Note that Δt_I is such that no numerical oscillations appeared (see Figure 6), and this is the motivation for using this as the internal time step. Nonetheless, the numerical scheme with time step Δt_E proved to be convergent throughout the iterations (see again Figure 6), so this is used as the external time step.

Figure 21 shows a comparison of the solution at the coupling point (i) when using a unique time step $\Delta t = 0.0005$ and (ii) when using the internal/external time steps combination. Notice that the solution does not exhibit the oscillations seen in Figure 6 in the wake of the wave. Then, as expected, the internal time step Δt_I remedied this numerical issue. Moreover, the external time step Δt_E proved to be convergent in this case, as can be seen in the number of iterations performed (and its comparison with the unique time step case) also presented in Figure 21.

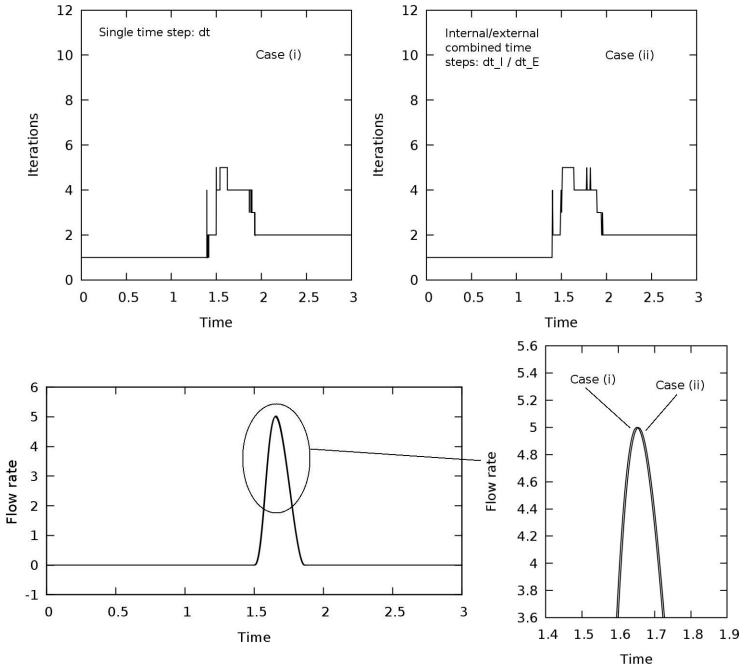

Figure 21: Solution at the coupling point. Comparison between the standard case when using a single time step (case (i)) and the internal/external combined time steps scheme (case (ii)) (simulation data: Broyden's method, $\Delta t = 0.0005$, $\Delta t_E = 0.005$, $\Delta t_I = 0.0005$, pressure boundary conditions everywhere, without inner iterations).

7. Conclusions

In this work a partitioned approach originally conceived to couple dimensionally-heterogeneous models was developed and successfully tested in the context of coupling black-box dimensionally-homogeneous (1D) blood flow models. This procedure exhibited high flexibility in relation to the arbitrariness in the setting of boundary conditions for the different partitions when compared with Gauss-Seidel-based methods, for which a hierarchy in the setting of boundary conditions should be established a priori. In addition, the results showed that the iterative strategies proposed here are suitable for the simulation of wave

propagation in compliant vessels with particular emphasis on its application to computational hemodynamics.

Comparisons of the performance of the iterative algorithms when considering different types of boundary information at the coupling interfaces and when modifying the time step were also presented. Moreover, the methodologies were applied to solve an extensive systemic network and to test the performance in a situation consisting of a physiological cardiovascular regime, for which the approach proved to perform effectively.

The results reported here suggest that the best choice for iterative coupling of 1D blood flow models, in terms of *solver–boundary condition* combination, consists of orthogonalized Broyden's method (with initialization) with pressure boundary conditions at all coupling points. If the simulation becomes unstable, the simple cure is to reduce the time step. In very extreme cases some additional stability can be gained by skipping the orthogonalization at the expense of slower convergence.

Acknowledgements

This work was partially supported by the Brazilian agencies CNPq and FAPESP. The support of these agencies is gratefully acknowledged.

References

[1] J. Alastruey, K. Parker, J. Peiró, S. Byrd, S. Sherwin, Modelling the circle of willis to assess the effects of anatomical variations and occlusions on cerebral flows, J. Biomech. 40 (2007) 1794–1805.

[2] A. Avolio, Multi–branched model of the human arterial system, Med. Biol. Engrg. Comp. 18 (1980) 709–718.

[3] P. Bruinsma, T. Arts, J. Dankelman, J. Spaan, Model of the coronary circulation based on pressure dependence of coronary resistance and compliance, Basic Res. Cardiol. 83 (1988) 510–524.

[4] L. Formaggia, D. Lamponi, A. Quarteroni, One-dimensional models for blood flow in arteries, J. Eng. Math. 47 (2003) 251–276.

[5] L. Formaggia, A. Quarteroni, A. Veneziani, Cardiovascular Mathematics, volume 1 of Modeling and simulation of the circulatory system (chapter 10), Springer, Milano, 2009.

[6] Y. Huo, G. Kassab, A hybrid one-dimensional/womersley model of pulsatile blood flow in the entire coronary arterial tree, Am. J. Physiol. Heart. Circ. Physiol. 292 (2007) H2623–H2633.

[7] R. Kufahl, M. Clark, A circle of Willis simulation using distensible vessels and pulsatile flow, J. Biomech. Engrg. 107 (1985) 112–122.

[8] M. Olufsen, Structured tree outflow condition for blood flow in larger systemic arteries, Am. J. Physiol. 276 (1999) H257–H268.

[9] M. Olufsen, C. Peskin, W. Kim, E. Pedersen, A. Nadim, J. Larsen, Numerical simulation and experimental validation of blood flow in arteries with structured-tree outflow conditions 28 (2000) 1281–1299.

[10] J. Reichold, M. Stampanoni, A. Keller, A. Buck, P. Jenny, B. Weber, Vascular graph model to simulate the cerebral blood flow in realistic vascular networks, J. Cereb. Blood Flow Metab. 29 (2009) 1429–1443.

[11] P. Reymond, F. Merenda, F. Perren, D. Rüfenacht, N. Stergiopulos, Validation of a one-dimensional model of the systemic arterial tree, Am. J. Physiol. Heart. Circ. Physiol. 297 (2009) H208–H222.

[12] B. Schaaf, P. Abbrecht, Digital computer simulation of human systemic arterial pulse wave transmission: A nonlinear model, J. Biomech. 5 (1972) 345–364.

[13] S. Sherwin, V. Franke, J. Peiró, K. Parker, One-dimensional modelling of a vascular network in space-time variables, J. Eng. Math. 47 (2003) 217–250.

[14] M. Snyder, V. Rideout, R. Hillestad, Computer modelling of the human systemic arterial tree, J. Biomech. 1 (1968) 341–353.

[15] N. Stergiopulos, D. Young, T. Rogge, Computer simulation of arterial flow with applications to arterial and aortic stenoses, J. Biomech. 25 (1992) 1477–1488.

[16] J. Wang, K. Parker, Wave propagation in a model of the arterial circulation, J. Biomech. 37 (2004) 457–470.

[17] R. Karch, F. Neumann, M. Neumann, W. Schreiner, A three-dimensional model for arterial tree representation, generated by constrained constructive optimization, Comput. Biol. Med. 29 (1999) 19–38.

[18] W. Schreiner, F. Neumann, M. Neumann, A. End, M. Müller, Structural quantification and bifurcation symmetry in arterial tree models generated by constrained constructive optimization, J. Theor. Biol. 180 (1996) 161–174.

[19] J. Leiva, P. Blanco, G. Buscaglia, Iterative strong coupling of dimensionally-heterogeneous models, Int. J. Num. Meth. Engng. 81 (2010) 1558–1580.

[20] P. Blanco, R. Feijóo, S. Urquiza, A unified variational approach for coupling 3D–1D models and its blood flow applications, Comp. Meth. Appl. Mech. Engrg. 196 (2007) 4391–4410.

[21] L. Formaggia, J. Gerbeau, F. Nobile, A. Quarteroni, On the coupling of 3D and 1D Navier–Stokes equations for flow problems in compliant vessels, Comp. Meth. Appl. Mech. Engrg. 191 (2001) 561–582.

[22] T. Hughes, On the one-dimensional theory of blood flow in the larger vessels, Mathematical Biosciences 18 (1973) 161–170.

[23] T. Moody, D. Barclay, R. Tait, A boundary value problem for fluid-filled viscoelastic tubes, Mathematical Modelling 4 (1983) 195–207.

[24] T. Moody, D. Barclay, S. Greenwald, Impulse propagation in liquid filled distensible tubes: theory and experiment for intermediate to long wavelengths, Acta Mechanica 59 (1986) 47–58.

[25] J. Dennis, R. Schnabel, Numerical Methods for Unconstrained Optimization and Nonlinear Equations, Classics in applied mathematics, SIAM, 1996.

[26] C. Kelley, Iterative Methods for Linear and Nonlinear Equations, Frontiers in applied mathematics, SIAM, 1995.

[27] S. Urquiza, P. Blanco, M. Vénere, R. Feijóo, Multidimensional modelling for the carotid artery blood flow, Comp. Meth. Appl. Mech. Engrg. 195 (2006) 4002–4017.

[28] S. Urquiza, M. Vénere, F. Clara, R. Feijóo, Finite element (one-dimensional) haemodynamic model of the human arterial system, in: Proceedings of the European Congress on Computational Methods in Applied Sciences and Engineering (ECCOMAS 2000), Barcelona, Dordrecht, 2000, pp. 1–13.

[29] S. Urquiza, Hemodinámica computacional del sistema arterial humano (in spanish), Ph.D. thesis, Instituto Balseiro, Centro Atómico Bariloche, Bariloche (2009).

[30] W. Nichols, M. O'Rourke, McDonald's Blood Flow in Arteries: Theoretical, Experimental and Clinical Principles, Arnold and Oxford University Press, 1998.

[31] M. Spencer, A. Denison, The square–wave electro–magnetic flowmeter: Theory of operation and design of magnetic probes for clinical and experimental applications, I.R.E. Trans. Med. Elect. 6 (1959) 220–228.